Analyst

PAPER

Cite this: *Analyst*, 2015, **140**, 7012

Illustration of SID-IM-SID (surface-induced dissociation-ion mobility-SID) mass spectrometry: homo and hetero model protein complexes†

Royston S. Quintyn,[a] Sophie R. Harvey[a,b] and Vicki H. Wysocki*[a]

The direct determination of the overall topology and inter-subunit contacts of protein complexes plays an integral role in understanding how different subunits assemble into biologically relevant multisubunit complexes. Mass spectrometry has emerged as a useful structural biological tool because of its sensitivity, high tolerance for heterogeneous mixtures and the fact that crystals are not required. Perturbation of subunit interfaces in solution followed by gas-phase detection using mass spectrometry is a current means of probing the disassembly and hence assembly of protein complexes. Herein, we present an alternative method that employs native mass spectrometry coupled with ion mobility and two stages of surface induced dissociation (SID) where protein complexes are dissociated into subcomplexes in the first SID stage. The subcomplexes are then separated by ion mobility and subsequently fragmented into their individual monomers in the second SID stage (SID-IM-SID), providing information on how individual subunits assemble into protein complexes with different native topologies. The results also illustrate complex dependent differences in charge redistribution onto individual monomers obtained in SID-IM-SID.

Received 2nd June 2015,
Accepted 27th August 2015

DOI: 10.1039/c5an01095k

www.rsc.org/analyst

Introduction

A host of cellular processes are mediated by the formation, and dynamic interaction, of macromolecular complexes.[1,2] Consequently, characterizing the quaternary structures of protein complexes and their assembly pathways constitutes a necessary step towards the mechanistic understanding of these cellular processes. There are several structural characterization techniques available, such as X-ray crystallography, small-angle X-ray scattering (SAXS), electron microscopy (EM) and nuclear magnetic resonance (NMR) spectroscopy that serve as powerful tools in probing the architecture of protein complexes.[3,4] However, these approaches are often limited due to the high quantities of sample required, need for very pure samples, and difficulty in studying conformationally dynamic systems.[5] The ability to characterize protein complex disassembly and hence assembly pathways has been greatly aided by the coupling of native mass spectrometry (MS) with ion mobility (IM), which can identify the different subcomplexes formed during solution-phase disassembly.[6] This is possible because subcomplexes generated from solution disruption typically resemble the native structures within the intact assembly.[7,8] The generation of subcomplexes from intact assemblies is also possible in the gas-phase by employing tandem mass spectrometry (MS/MS).[9] However, the most common dissociation method utilized in MS/MS experiments, collision induced dissociation (CID), provides limited direct information on subunit arrangement in the native complex as it typically results in "asymmetric" dissociation into highly charged monomers and complementary (n-1)-mers as the complex undergoes multiple collisions with a neutral gas.[10]

Alternatively, surface induced dissociation (SID), which involves collision with a surface target, has been shown to yield products reflective of the complex topology, as it allows for the structurally informative, direct dissociation pathways to outcompete the multistep monomer unfolding dissociation pathway.[10] Consequently, prior studies published by the Wysocki group have been successful in utilizing SID as a means of dissociating protein complexes to subcomplexes to facilitate the mapping of subunit contacts within protein complexes, thereby generating direct information on their quaternary structure.[11,12] Moreover, we have also demonstrated that low-energy SID of D_2 homotetramers (complexes with dihedral

[a]*Department of Chemistry and Biochemistry, Ohio State University, 484 W. 12th Ave., Columbus, Ohio 43210, USA. E-mail: wysocki.11@osu.edu*
[b]*School of Chemistry, Manchester Institute of Biotechnology, University of Manchester, Manchester, M1 7DN, UK*

†Electronic supplementary information (ESI) available. See DOI: 10.1039/c5an01095k

symmetry[7]) initially results in cleavage of the smaller dimer–dimer interfaces yielding C_2 dimers (complexes with cyclic symmetry), whereas higher-energy SID results in the secondary cleavage of the larger monomer–monomer interface within the C_2 dimer to produce monomers. These results allowed us to conclude that the SID dissociation pathway (D_2 tetramer → C_2 dimer → monomer) is the reverse of the known assembly pathway.[13] The deconvolution of assembly pathways by SID energy-resolved MS (SID-ERMS) requires monitoring the relative intensities of all SID products (including indirect secondary fragments) obtained from multiple experiments conducted at various SID collision energies and then plotting the relative intensity of the precursor and all products as a function of SID energy producing a SID-ERMS plot. Therefore, although the use of SID-ERMS plots is a relatively straightforward and useful strategy for simple systems such as D_2 homotetramers, interpretation of primary *vs.* secondary products in these plots becomes more difficult when studying more complex heterogeneous systems from which many possible subcomplexes can be produced and, hence, many possible indirect secondary fragments can also be derived.

Based on the results described earlier for solution disruption/MS and our single stage SID experiments, we hypothesize that by first generating subcomplexes by SID, followed by IM separation and the direct dissociation of these subcomplexes to individual subunits, it may be possible to probe the relationship between the disassembly and quaternary structure of a protein complex in direct experiments. The present study seeks to test this hypothesis by modifying a quadrupole/IM/time-of-flight (Q/IM/TOF) instrument to incorporate two customized SID devices (before and after the IM chamber) to allow for two stages of SID dissociation followed by detection of the products, after separation, in the TOF. We introduce a method to generate subcomplexes by low energy trap SID (Scheme 1a), which has been shown to proceed *via* cleavage of the smallest interface(s) within the complexes first. The SID products are then separated by size, shape and charge in IM,[14,15] following which they can be further dissociated (into individual subunits) by higher energy SID within the transfer region (transfer SID), as shown in Scheme 1b.

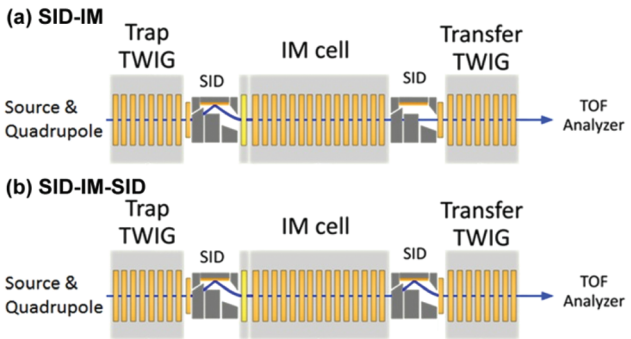

Scheme 1 T-wave region of the modified Waters Synapt G2-S instrument showing the (a) SID-IM and (b) SID-IM-SID experiments.

Results and discussion

Three model complexes with different native topologies were chosen for this initial, proof of concept, investigation: streptavidin, a homotetramer that is a dimer of dimers, tryptophan synthase, a heterotetramer with a somewhat linear αββα arrangement, and the homopentamer C-reactive protein, which has cyclic symmetry. Streptavidin (SA) was recently used in our assembly/disassembly studies of D_2 homotetramers described elsewhere,[13] making it an appealing model system for this SID-IM-SID investigation. The dissociation behavior observed in trap CID (Fig. 1a, tetramer → monomer + trimer) and trap SID (Fig. 1b, tetramer → dimer) is similar to that observed in our previous assembly/disassembly studies involving the SA tetramer.[13] Because trap CID and SID occur before the IM cell, the different products are separated within the IM cell and hence have unique drift times, with predicted *m*/*z* of streptavidin subcomplexes given in Table S1.† Comparison of the CID-IM and SID-IM results (Fig. 1a and b respectively and Table S2†) shows several clear differences. The spectra show the dissociation observed at the energies at which dissociation is first observed, CID 1430 eV and SID 330 eV. A significantly lower energy is required to dissociate the ions with SID in comparison to CID. This is due to a number of factors, with SID dissociation occurring following a collision event with a massive target (surface) in which the energy is rapidly deposited. In CID, the ions undergo multiple, stepwise collisions with much smaller targets (gaseous Ar). This stepwise dissociation involves a range of impact parameters and CID typically requires larger lab frame kinetic energies to dissociate ions than does SID. Furthermore, the undissociated +11 SA tetramer in CID experiments spends a significantly longer time in the IM cell (14.51–19.40 ms) than the native +11 SA tetramer in MS experiments (10.88–11.79 ms) and has a broader range of drift times, indicative of unfolding of the SA tetramer in CID. Therefore, these results confirm that the unfolding typically associated with CID and the corresponding inability to generate informative subcomplexes is responsible for its inability to directly give information on the quaternary structure of protein complexes. In contrast, the majority of undissociated SA tetramer from SID-IM has a similar drift time to the native SA tetramer in MS experiments. However, using single stage SID alone, we cannot completely rule out the possibility that a fraction of the undissociated tetramers with similar CCS as the original tetramer may be due to the tetramer not colliding with the surface. Instead, further fragmentation of that undissociated tetramer (see below) is needed, as it may provide evidence that the tetramers have been activated by a surface collision. Although the dominant *monomers* in CID are clearly unfolded (experimental CCS of 17.10 nm^2 (Table S2†) *vs.* 15.27 nm^2 expected CCS for a monomer clipped from the crystal structure), the average experimental CCS obtained for the SID *dimer* fragments (20.96 nm^2 ± 0.06 nm^2, Table S2†) is similar to the theoretical CCS calculated for the dimers (20.98 nm^2 for a dimer clipped from the crystal structure). Hence, as previously reported, SID of SA results in dissociation

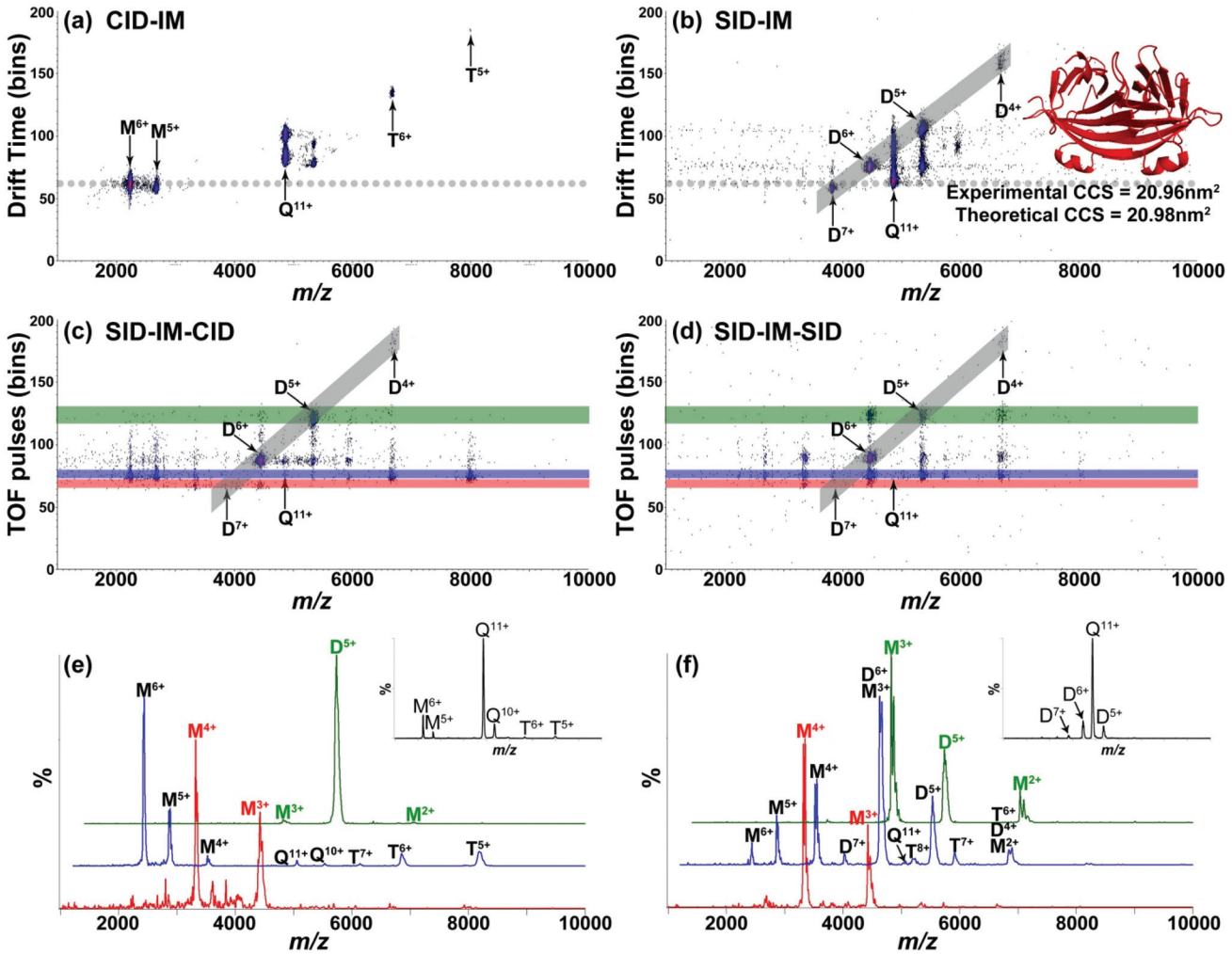

Fig. 1 Ion mobilogram plots showing (a) CID-IM and (b) SID-IM of the +11 SA tetramer at collision energies (CE) of 1430 eV and 330 eV respectively. The SA dimer clipped from the crystal structure of SA for comparison with the dimer produced by dissociation of a D_2 tetramer is shown in the inset of (b). The grey dotted line represents the TOF pulse in which the native +11 SA tetramer appears in MS experiments. Ion mobilogram showing the fragments produced in (c) SID-IM-CID and (d) SID-IM-SID experiments are also shown. Trap SID CE is 330 eV and the transfer CID and SID CEs are 1650 eV and 1320 eV, respectively, for tetramer (blue), 1050 eV and 840 eV for +7 dimer (red), and 750 eV and 600 eV for +5 dimer (green). The MS/MS spectra extracted from the highlighted regions of the SID-IM-CID and SID-IM-SID are shown in (e) and (f) respectively. The insets show representative MS/MS spectra from lower energy SID-IM-CID and SID-IM-SID of the remaining +11 SA tetramer from initial SID-IM (CE = 330 eV). Extracted MS/MS spectra are color coded to represent their corresponding highlighted regions in the SID-IM-CID/SID mobilograms (green (top), blue (middle) and red (bottom) in each case). M, D, T and Q represent monomer, dimer, trimer and tetramer respectively. The ion mobilogram plots are shown on a square root scale.

patterns that are reflective of the quaternary structure of the native protein complex.[13]

Next, we employed a second stage of dissociation, either CID or SID, to fragment the products obtained from initial SID-IM. Fig. 1c (SID-IM-CID) and 1d (SID-IM-SID) represent experiments where primary SID products of the +11 SA tetramer (*e.g.*, those obtained in 1b) are separated by IM and allowed to further fragment by CID or SID. Because the dimers produced from low-energy trap SID (330 eV) of the +11 SA tetramer are formed before the IM cell, they are separated in the IM cell and appear in separate TOF pulses (highlighted by the grey diagonal line). However, the fragments produced from transfer CID and SID are formed after the IM, and thus appear in identical TOF pulses along with the dimers from which they are generated. Therefore, by taking horizontal slices of the mobilogram plots shown in Fig. 1c and d, we can extract the MS/IM/MS spectra and successfully identify the fragments produced from the direct dissociation of the mobility separated dimers and undissociated tetramer. It should be noted that in order to extract these data the species have to be well separated in IM, in order to obtain the spectra for a single subcomplex. Fig. 1e and f illustrate extracted spectra corresponding to fragmentation of different primary (SID-IM) products, with red (bottom trace) corresponding to fragmentation of +7 dimer, green (top trace) corresponding to fragmentation of +5 dimer, and blue (middle trace) corresponding to fragmentation of +11

tetramer. It is immediately apparent that the more highly charged +7 dimer (7 × 120 V = 840 eV in SID) fragments much more completely than the +5 dimer (5 × 120 V = 600 eV in SID). Dissociation of the +7 dimer, which is produced by asymmetric charge partitioning of the initial +11 tetramer (+11 tetramer → +7 & +4 dimers) yields +3 and +4 monomers in both SID-IM-CID and SID-IM-SID. In contrast the +5 dimer produced by symmetric charge partitioning of the +11 tetramer (+11 tetramer → +6 & +5 dimers) yields +2 and +3 monomers, which better correlates with the expected charge state of monomers generated from symmetric dissociation of an +11 tetramer (+11/4 monomers = +2.75/monomer). Although both SID-IM-CID and SID-IM-SID result in symmetric dissociation of dimers, the energy onset at which dissociation of the +5 dimer is observed in CID (Fig. 2a, 550 eV) is significantly higher than that in SID (Fig. 2b, 300 eV) and the extent of dissociation in CID is much lower. This suggests that SID-IM-SID is a more effective means of directly dissociating subcomplexes (generated in SID-IM) into their individual subunits than SID-IM-CID, as is also shown for the +6 dimer (Fig. 1c and d).

Moreover, as illustrated in Fig. 1e and f (blue spectra) SID-IM-CID of the remaining +11 SA tetramer yields highly charged monomer (+5,+6) and complementary trimer (+6,+5), whereas SID-IM-SID yields predominantly lower-charged dimers (+5,+6) and monomers (+3,+4). Previous studies revealed that high energy SID of the SA tetramer results in primary cleavage to dimers and secondary cleavage of the larger monomer–monomer interface within the dimer to produce monomers.[13] Therefore, we speculate that high abundance of lower-charged monomers is due to the high SID-IM-SID energy (1320 eV for second stage SID). This speculation is further confirmed by the fact that lower energy SID-IM-SID (inset of Fig. 1f, 550 eV for second stage SID) of the undissociated +11 SA tetramer from trap SID yields primarily dimer. These results indicate that SID-IM-SID serves as a means of probing the relationship between the disassembly and quaternary structure of a protein complex in more direct experiments than is possible with SID-IM or SID-IM-CID. Based on the streptavidin results, SID-IM-SID offers the distinct advantage of enabling each subcomplex to be interrogated individually within a single experiment and, therefore, can directly confirm the proposed dissociation pathway.

As noted above, the majority of the undissociated SA tetramer from SID-IM has a drift time similar to that of the native SA tetramer. SID-IM-SID thus provides an opportunity to probe whether the undissociated precursor has indeed collided with the surface. The undissociated tetramer from SID-IM was, therefore, further fragmented in SID-IM-SID over a range of collision energies to determine whether the entire fraction of +11 SA tetramer collides with the surface in single stage SID dissociation. An ERMS plot was generated by extracting the spectra corresponding to the +11 SA tetramer with similar CCS as the original tetramer (TOF pulses: 60–65 bins) and the fraction of remaining precursor was determined. A comparison of the fragmentation efficiency plot generated for the +11 SA tetramer from SID-IM and SID-IM-SID experiments (Fig. 2c)

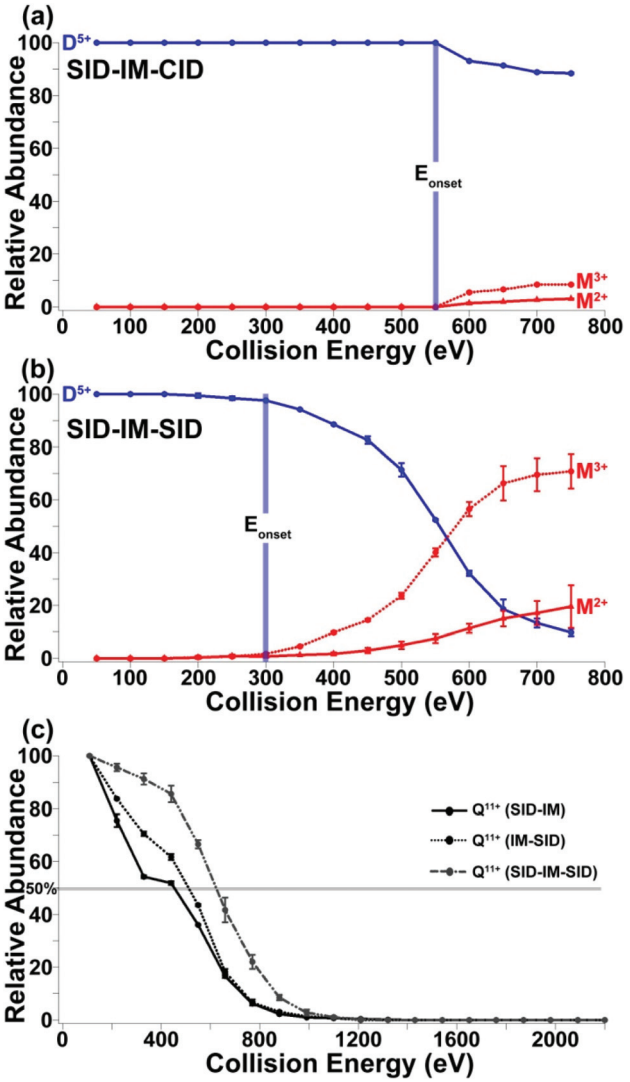

Fig. 2 (a) SID-IM-CID and (b) SID-IM-SID fragmentation efficiency plot of +5 dimer initially produced from SID-IM of the +11 SA tetramer (CE = 330 eV). (c) SID-IM, IM-SID and SID-IM-SID fragmentation efficiency plots of the +11 SA tetramer. All ERMS plots represent the average from two repeats. The CE of the first stage SID in the SID-IM-SID experiments was 330 eV. E_{onset} represents the collision energy where dissociation is first observed. M, D and Q represent monomer, dimer and tetramer respectively.

clearly illustrates that more SID collision energy is needed to fragment 50% of the undissociated "native-like" SA tetramer in SID-IM-SID (625 eV for second stage SID) as compared with the unactivated SA tetramer in single-stage SID-IM dissociation (455 eV). However, we considered that this increase might also be due to annealing in the IM cell, as the undissociated +11 SA tetramer passes through the IM cell before it can undergo SID-IM-SID. Single stage IM-SID experiments (where the unactivated precursor also passes through the IM cell before SID dissociation) were subsequently conducted to determine the effects of annealing. Although annealing leads to an increase in the SID collision energy needed to fragment 50% of the

+11 SA tetramer (510 eV in IM-SID *vs.* 455 eV in SID-IM), the change is relatively small when compared with that observed in SID-IM-SID (625 *vs.* 455 eV). Therefore, the results confirm that the undissociated +11 SA tetramer has collided with the surface with no significant change in CCS. We speculate that in addition to the conformational changes associated with annealing in the IM cell, the undissociated +11 SA tetramer also undergoes a structural change upon activation (in spite of the lack of change of CCS), which may explain the increase in SID collision energy required for dissociation. We have also seen this behavior in source-activated protein complexes. These changes may be measureable in future if higher resolution IM can be coupled to SID.

Non-identical subunits can also interact to form heteromeric complexes, and a large fraction of proteins participate in heteromeric protein–protein interactions *in vivo*.[16] Because heteromeric complexes have different types of subunits, the range of quaternary structures they might adopt is greater than is possible for homomeric complexes.[17] However, previous studies published in the literature have demonstrated that the assembly of both homomeric and heteromeric complexes is driven by a hierarchy of interface size, with subcomplexes assembled in the initial stages possessing the largest interfaces.[7,8] Therefore, we decided to utilize SID-IM-SID to probe the relationship between quaternary structure and disassembly of the model heterotetramer tryptophan synthase (TS). The native topology of the TS tetramer can be described as four subunits arranged in an almost linear fashion to form an αββα complex.[18] In order to determine whether the disassembly of the TS tetramer is driven by a hierarchy of interface size, we first calculated the interfacial surface area of the α/β (1363 Å^2) and β/β (1624 Å^2) interfaces using PISA analysis.[19] Low-energy SID-IM (570 eV, Fig. 3a) of the charge-reduced +19 TS tetramer results in the disruption of the smaller α/β interface to yield α-monomer and its complementary $\alpha\beta_2$-trimer, with predicted *m*/*z* of TS subcomplexes given in Table S3.† SID-IM at an intermediate SID collision energy (Fig. 3b, 1330 eV) results in a variety of products that are representative of the quaternary structure of TS. For example, in addition to the dominant products α-monomer and ββα-trimer, the detection of a minor amount of β_2-dimer indicates that the two β subunits are connected. Further, the presence of an $\alpha\beta_2$-trimer coupled with the fact that an α_2-dimer is not observed is consistent with the β_2-dimer being flanked by the α subunits.

Next, we utilized SID-IM-SID as a means of fragmenting the $\alpha\beta_2$-trimer and β_2-dimer with the aim of illustrating that more information can be gained on the assembly of TS tetramer. It is necessary, however, to consider that the $\alpha\beta_2$-trimer may not have the same structure as the trimer clipped from the crystal structure, as the CCS of the trimer produced in SID-IM experiments (58.83 nm^2) is much smaller than the CCS obtained for the trimer clipped from the crystal structure (66.67 nm^2). SID-IM-SID of $\alpha\beta_2$-trimer (Fig. 3c) produced from initial SID-IM results in the disruption of the other α/β interface yielding α-monomer and β_2-dimer, consistent with the interfacial analysis in which the α/β was calculated to be smaller than the β/β interface. In addition, SID-IM-SID of the β_2-dimer fragment, from initial SID-IM, results in disruption of the β/β interface to produce β-monomers as expected (Fig. 3d). It is

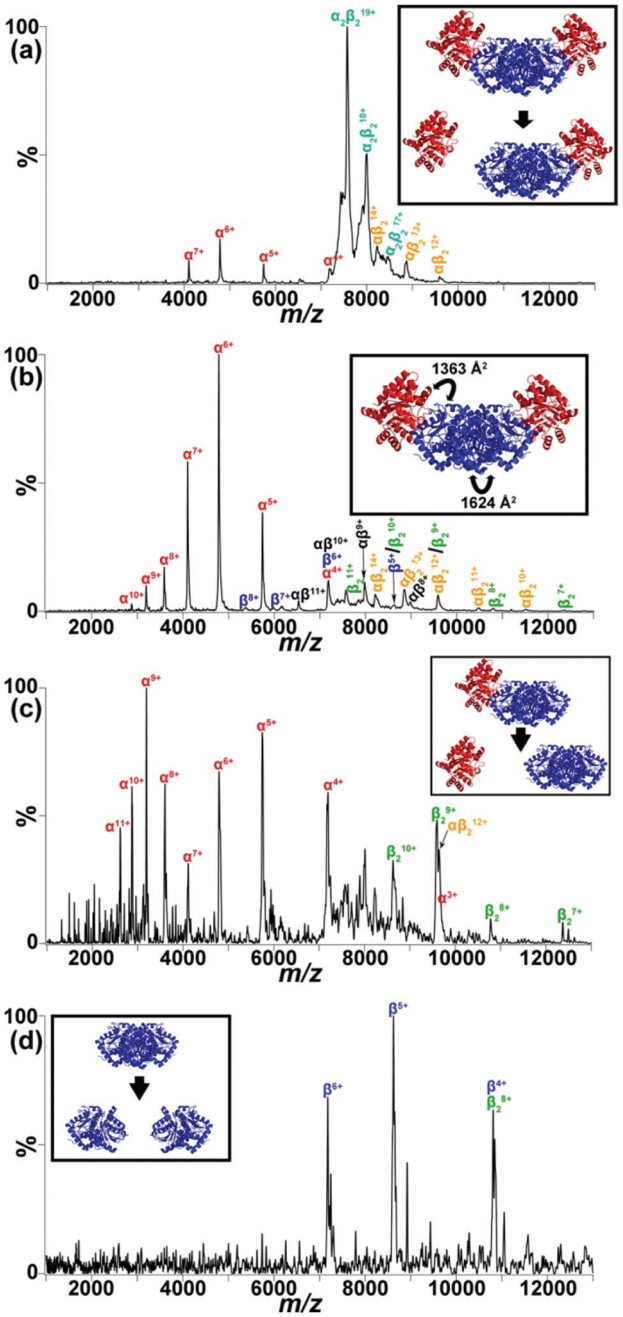

Fig. 3 (a) SID spectrum resulting from low energy SID-IM of +19 αββα TS tetramer at a collision energy of 570 eV. The dominant dissociation pathway is shown in the inset along with the crystal structure (PDB code: 1WBJ) (b) SID spectrum showing the different charged fragments produced from the SID-IM of the +19 αββα TS tetramer at a collision energy of 1330 eV. The corresponding interfacial areas calculated from the TS crystal structure are given in the inset. SID-IM-SID (CE for second stage SID = 2280 eV) of the (c) +12 $\alpha\beta_2$-trimer and (d) +8 β_2-dimer initially produced from SID-IM (CE = 1330 eV) of the +19 αββα TS tetramer. The possible dissociation pathways of the +12 $\alpha\beta_2$-trimer and +8 β_2-dimer are shown in the inset of (c) and (d) respectively.

interesting to note that the experimental CCS of the β_2-dimer (47.82 nm^2 ± 0.44 nm^2) is similar although slightly more compact than the theoretical CCS (51.22 nm^2). Consequently, SID-IM-SID results predict that the assembly of the TS tetramer is a three-step process, where the larger β/β interface is formed by the interaction of two β subunits, followed by the association of the α-monomer and β_2-dimer to form one of the α/β interfaces. The final step involves the binding of another α-monomer to the $\alpha\beta_2$-trimer to form the αββα TS tetramer. The TS assembly pathway proposed here, based upon results of our SID-IM and SID-IM-SID experiments, is in excellent agreement with other descriptions of the self-assembly of the TS complex.[8,20,21]

One difference between the SID-IM-SID results of SA and TS is the charge of the product ions. Streptavidin shows charge conservation with +11 tetramer fragmenting to +6 and +5 dimers, which fragment to +3 and +3 or +3 and +2 monomers, respectively, as expected if charge is conserved on product ions. The initial fragmentation of +19 TS gives +5 to +7 α-monomer and +12 to +14 $\alpha\beta_2$-trimer, a result that seems reasonable for a heterotetramer. High energy SID of the +12 $\alpha\beta_2$-trimer in the SID-IM-SID experiment surprisingly leads to two distributions of α-monomer, one centered around +9 (likely an extended population) and the other at +5 (presumably compact). The highly charged monomer is consistent with significant structural rearrangement, or unfolding, and charge transfer from the trimer. Previous studies have shown, in a complex dependent manner, that SID product ions can be collapsed, even when folded monomers are produced and even when folded monomers make up a higher order oligomer.[22] The highly charged products may also be due to the high energy second stage of SID used here. In order to further probe the extent of charge conservation in SID-IM-SID an additional protein complex C-reactive protein (CRP) was studied.

C-reactive protein (CRP) is a cyclic pentameric assembly of identical non-covalently associated subunits,[23] with PISA analysis determining that the interfacial surface area between all monomeric subunits is similar, with predicted *m*/*z* of CRP subcomplexes given in Table S4.† Trap SID of the charge-reduced +18 CRP pentamer (Fig. 4a) yields primarily monomers and a small amount of all possible subcomplexes (dimers, trimers and tetramers), an SID result that is common for ring-shaped homooligomers. The experimental CCS of the dimers obtained here from trap SID (30.09 nm^2 ± 0.35 nm^2) is close to the theoretical CCS (32 nm^2) calculated using two adjacent monomers clipped from the CRP crystal structure (1GNH).

The "native-like" dimers produced from trap SID of the CRP pentamer were then further fragmented by a second stage of SID, producing monomers with symmetric charge partitioning (Fig. 4b). The dissociation of +7 dimer → +3 & +4 monomers allows us to propose that the dimer comprises two folded monomers, and that the charge is conserved on the individual subunits from pentamer → dimer → monomer. As shown in previous SID-IM studies,[24] the larger protein subunits derived from trap SID of the CRP pentamer in the present study are

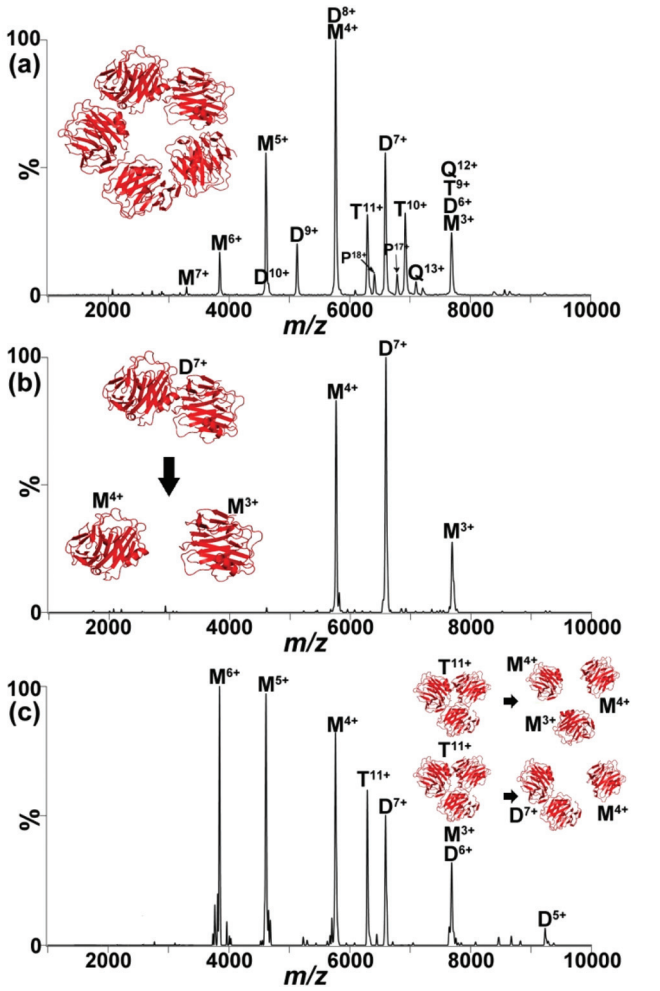

Fig. 4 (a) SID spectrum showing the different charged fragments produced from the trap SID of the +18 CRP pentamer at a collision energy of 1260 eV. The crystal structure of CRP (PDB code: 1GNH) is shown in the inset. Transfer SID (CE = 2160 eV) of the (b) +7 CRP dimer and (c) +11 CRP trimer produced from trap SID (CE = 1260 eV) of the +18 CRP pentamer. Selected possible dissociation pathways of the +7 dimer and +11 trimer are shown in the inset of (b) and (c) respectively.

present as compact, potentially collapsed, structures. Unlike the dimers, the experimental CCS of the trimers obtained from trap SID (39.39 nm^2 ± 0.42 nm^2) is significantly different from the theoretical CCS (46 nm^2) calculated using three adjacent monomers clipped from the CRP crystal structure. However, the experimental CCS of the trimers shows a somewhat better correlation with the theoretical CCS calculated for the collapsed trimer shown in the inset of Fig. 4c (43 nm^2), which was generated by rearranging the monomers into a more compact structure as might be expected of a subcomplex seeking intramolecular charge and structure stabilization.

The +11 CRP trimer formed by the initial trap SID of pentamer was also subjected to the second stage transfer SID and the fragment ions produced are illustrated in Fig. 4c. The presence of both low and high charged monomers suggests that

there may be multiple competing dissociation pathways. For example, the presence of +3 and +4 monomers allowed us to speculate that one possible dissociation pathway is: +11 CRP trimer → +3, +4 and +4 monomers. Another possible dissociation pathway is: +11 CRP trimer → +4 monomer and +7 dimer, which may suggest that all the monomer-monomer interfaces in the compact trimer obtained from trap SID are similar. These dissociation pathways show conservation of charges from the initial precursor throughout the SID-IM-SID process, as was seen for SA. Interestingly, transfer SID of the +11 CRP trimer also results in asymmetric charge partitioning between monomers and dimers (+11 trimer → +6 monomer & +5 dimer and +11 trimer → +5 monomer & +6 dimer). We speculate that this dissociation pathway is possible because very high SID energies were used and that allows all possible dissociation pathways (including the rearrangement pathway, which leads to the unfolding and ejection of a more highly charged monomer; this pathway may increase in probability when the altered structure trimer collides with the surface).

Experimental

Chemicals and reagents

Streptavidin and recombinant human C-reactive protein from *E. coli* were purchased from Thermo Scientific Pierce Biotechnology (Rockford, IL, U.S.A.) and Calbiochem (San Diego, CA, U.S.A.), respectively. Tryptophan Synthase, ammonium acetate (AA) and triethyl ammonium acetate (TEAA) were purchased from Sigma-Aldrich (St. Louis, MO, U.S.A.). All samples were buffer exchanged into 100 mM ammonium acetate (pH 7) using 6 kDa cut-off Micro Bio-Spin 6 columns from Bio-Rad (Hercules, CA, U.S.A.), and analyzed in a 20 mM : 80 mM TEAA : AA electrospray buffer.

MS experiments

All experiments were conducted by utilizing a modified Q-IM-TOF instrument (Synapt G2-S, Waters Corp., Manchester, U.K.) with customized SID devices installed both before and after the IM chamber (see Scheme 1). Typical instrumental conditions are as follows: capillary voltage of 1.0–1.2 kV, cone voltage of 20 V, source offset voltage of 20 V, 2.4 mbar gas pressure in the IM cell, a gas flow rate of 120 mL min^{-1} into the helium cell and 4 mL min^{-1} into trap and transfer regions (in SID experiments- 2 mL min^{-1}) and a TOF analyzer pressure of $\sim 6 \times 10^{-7}$ mbar. Wave conditions in the IM cell were wave velocity: 300 ms^{-1} and wave height: 20 V.

Determination of collision cross section

The theoretical collision cross section (CCS) values were calculated from crystal structures using the Projection Approximation (PA) model[25] implemented in the open source software MOBCAL. The CCS values obtained were corrected as previously described[26] because the PA model typically underestimates CCS by approximately 14%.[27]

In a typical ion mobility measurement in the Synapt G2-S instrument, ions from the Trap TWIG are first injected into the IM cell and then separated into 200 bins based on their size, shape or charge. Each bin is subsequently pulsed separately into the TOF analyzer. Because of the non-linear electric field in the IM cell, the experimental CCS has to be externally calibrated rather than using measured drift times to directly calculate them. First the drift times of four standard calibrants (transthyretin, concanavalin A, serum amyloid P and glutamate dehydrogenase) with a mass range that brackets the mass of the analyte were obtained, and a linear calibration curve of the corrected drift time *vs.* the known CCS is generated. The corrected drift time is then determined for the analyte under identical instrument conditions as used for the standard calibrants, and the experimental CCS of the analyte is determined using the calibration curve.

Conclusion

In conclusion, SID-IM-SID can be utilized to probe the relationship between quaternary structure and disassembly of protein complexes, with assembly information inferred from the disassembly pathway. We applied this approach to fragment three model systems with different native topologies- a dimer of dimers (SA), a heterotetramer (TS) that is arranged in a linear αββα fashion, and a cyclic pentamer C-reactive protein (CRP). The results show how monomers associate to form subcomplexes, which then interact with each other to produce the complete protein complex. Furthermore, charge can be tracked, from precursor to products in a complex dependent manner in SID-IM-SID and is conserved in the fragmentation of some complexes (*e.g.* SA). The lack of charge conservation may be indicative of structural rearrangement, although more work is needed in this area.

Acknowledgements

We are grateful for financial support from the National Science Foundation (NSF DBI 1455654 to VHW). SRH is supported by a UK Engineering and Physical Sciences Research Council (EPSRC) Doctoral Prize Fellowship. The authors would like to thank Mike Morris and Kevin Giles of Waters Corporation, for helpful discussions in implementing SID-IM-SID. We are grateful to Waters Corporation for machining the two SID devices. Mowei Zhou is also thanked for his work in the initial stages of this project.

References

1 L. M. Veenhoff, E. H. M. L. Heuberger and B. Poolman, *Trends Biochem. Sci.*, 2002, **27**, 242–249.
2 P. Maurice, M. Kamal and R. Jockers, *Trends Pharmacol. Sci.*, 2011, **32**, 514–520.
3 D. L. Minor Jr., *Neuron*, 2007, **54**, 511–533.

4 A. B. Ward, A. Sali and I. A. Wilson, *Science*, 2013, **339**, 913–915.
5 C. V. Robinson, A. Sali and W. Baumeister, *Nature*, 2007, **450**, 973–982.
6 H. Hernández and C. V. Robinson, *Nat. Protoc.*, 2007, **2**, 715–726.
7 E. D. Levy, E. B. Erba, C. V. Robinson and S. A. Teichmann, *Nature*, 2008, **453**, 1262–1265.
8 J. A. Marsh, H. Hernández, Z. Hall, S. E. Ahnert, T. Perica, C. V. Robinson and S. A. Teichmann, *Cell*, 2013, **153**, 461–470.
9 A. J. R. Heck, *Nat. Methods*, 2008, **5**, 927–933.
10 R. L. Beardsley, C. M. Jones, A. S. Galhena and V. H. Wysocki, *Anal. Chem.*, 2009, **81**, 1347–1356.
11 A. E. Blackwell, E. D. Dodds, V. Bandarian and V. H. Wysocki, *Anal. Chem.*, 2011, **83**, 2862–2865.
12 M. Zhou, C. M. Jones and V. H. Wysocki, *Anal. Chem.*, 2013, **85**, 8262–8267.
13 R. S. Quintyn, J. Yan and V. H. Wysocki, *Chem. Biol.*, 2015, **22**, 583–592.
14 A. A. Shvartsburg and R. D. Smith, *Anal. Chem.*, 2008, **80**, 9689–9699.
15 S. D. Pringle, K. Giles, J. L. Wildgoose, J. P. Williams, S. E. Slade, K. Thalassinos, R. H. Bateman, M. T. Bowers and J. H. Scrivens, *Int. J. Mass Spectrom.*, 2007, **261**, 1–12.
16 K. Tarassov, V. Messier, C. R. Landry, S. Radinovic, M. M. S. Molina, I. Shames, Y. Malitskaya, J. Vogel, H. Bussey and S. W. Michnick, *Science*, 2008, **320**, 1465–1470.
17 T. Perica, J. A. Marsh, S. L. Filipa, E. Natan, L. J. Colwell, S. E. Ahnert and S. A. Teichmann, *Biochem. Soc. Trans.*, 2012, **40**, 475–491.
18 C. C. Hyde, S. A. Ahmed, E. A. Padlan, E. W. Miles and D. R. Davies, *J. Biol. Chem.*, 1988, **263**, 17857–17871.
19 E. Krissinel and K. Henrick, *J. Mol. Biol.*, 2007, **372**, 774–797.
20 A. N. Lane, C. H. Paul and K. Kirschner, *EMBO J.*, 1984, **3**, 279–287.
21 A. Ehrmann, K. Richter, F. Busch, J. Reimann, S.-V. Albers and R. Sterner, *Biochemistry*, 2010, **49**, 10842–10853.
22 M. Zhou, S. Dagan and V. H. Wysocki, *Analyst*, 2013, **138**, 1353–1362.
23 A. K. Shrive, G. M. T. Gheetham, D. Holden, D. A. A. Myles, W. G. Turnell, J. E. Volanakis, M. B. Pepys, A. C. Bloomer and T. J. Greenhough, *Nat. Struct. Mol. Biol.*, 1996, **3**, 346–354.
24 M. Zhou, S. Dagan and V. H. Wysocki, *Angew. Chem., Int. Ed.*, 2012, **51**, 4336–4339.
25 E. Mack, *J. Am. Chem. Soc.*, 1925, **47**, 2468–2482.
26 Z. Hall, A. Politis, M. F. Bush, L. J. Smith and C. V. Robinson, *J. Am. Chem. Soc.*, 2012, **134**, 3429–3438.
27 A. A. Shvartsburg and M. F. Jarrold, *Chem. Phys. Lett.*, 1996, **261**, 86–91.